

# Supplementary Information for Intramolecular Subtleties in Indole Azo Dyes Revealed by Multidimensional Potential Energy Surfaces

Allen H. Chen, Zachary J. Knepp, Christian A. Guzman, Elizabeth R. Young\*, Lisa A. Fredin\*

Department of Chemistry, Lehigh University, 6 E. Packer Ave., Bethlehem, PA 18015, USA

\*E-mail: ery317@lehigh.edu; lafredin@lehigh.edu

## Contents

<b>1 Synthesis and Experimental Results</b>	<b>S2</b>
<b>2 Quantum Mechanical Calculations</b>	<b>S11</b>
2.1 Optimized Structures . . . . .	S11
2.2 Transition States with Displacement Vectors . . . . .	S15
2.3 Method Comparison for Excited State Scan Calculations . . . . .	S19
2.4 Potential Energy Surfaces . . . . .	S21
2.5 Estimated Activation Energies . . . . .	S30
<b>3 TDDFT Tables</b>	<b>S31</b>

## List of Figures

S1 Schematic representation of all the rotamers of OMe-PAI and OMe-PAI-Ph . . . . .	S2
S2 $^1\text{H}$ NMR of <i>trans</i> -OMe-PAI . . . . .	S3
S3 $^1\text{H}$ NMR of <i>cis</i> -OMe-PAI . . . . .	S4
S4 $^1\text{H}$ NMR of <i>trans</i> -OMe-PAI-Ph . . . . .	S5
S5 $^1\text{H}$ NMR of <i>cis</i> -OMe-PAI-Ph . . . . .	S5
S6 $^1\text{H}$ - $^1\text{H}$ NOESY of <i>trans</i> -OMe-PAI (500 MHz, DMF, -30°C) . . . . .	S6
S7 $^1\text{H}$ - $^1\text{H}$ NOESY of <i>cis</i> -OMe-PAI (500 MHz, DMF, -30°C) . . . . .	S7
S8 $^1\text{H}$ - $^1\text{H}$ NOESY of <i>trans</i> -OMe-PAI-Ph (500 MHz, DMF, -30°C) . . . . .	S8
S9 $^1\text{H}$ - $^1\text{H}$ NOESY of <i>cis</i> -OMe-PAI-Ph (500 MHz, DMF, -30°C) . . . . .	S9
S10 Room temperature (25°C) and -30°C NMR of OMe-PAI-Ph (500 MHz, DMF) . . . . .	S10
S11 Four optimized meta-stable rotamers of OMe-PAI . . . . .	S11
S12 Four optimized meta-stable rotamers of OMe-PAI-Ph . . . . .	S12
S13 Molecular orbitals of OMe-PAI . . . . .	S13
S14 Molecular orbitals of OMe-PAI-Ph . . . . .	S14
S15 OMe-PAI TS structures . . . . .	S15
S16 OMe-PAI isorotamer TS structures . . . . .	S16
S17 OMe-PAI-Ph TS structures . . . . .	S17
S18 OMe-PAI-Ph isorotamer TS structures . . . . .	S18
S19 PEC excited state methods . . . . .	S20
S20 Discontinuity on $S_0$ PEC . . . . .	S21
S21 PEC at CNNC $\approx$ 90° . . . . .	S26
S22 PECs including $T_1$ . . . . .	S28
S23 <i>anti-trans</i> $\rightarrow$ <i>anti-cis</i> $\rightarrow$ <i>eclipsed-cis</i> of OMe-PAI . . . . .	S28
S24 <i>anti-trans</i> $\rightarrow$ <i>anti-cis</i> $\rightarrow$ <i>eclipsed-cis</i> of OMe-PAI-Ph . . . . .	S29

## List of Tables

S1	Experimental isomerization lifetimes . . . . .	S3
S2	Energies (eV) for OMe-PAI and OMe-PAI-Ph . . . . .	S11
S3	CCSD(T) vs. DFT energies in MeCN . . . . .	S12
S4	CCSD(T) vs. DFT energies of OMe-PAI-Ph in DMF . . . . .	S12
S5	<i>Ind</i> CNN OMe-PAI PES energies . . . . .	S21
S6	<i>Ph</i> CNN OMe-PAI PES energies . . . . .	S23
S7	<i>Ind</i> CNN OMe-PAI-Ph PES energies . . . . .	S24
S8	<i>Ph</i> CNN OMe-PAI-Ph PES energies . . . . .	S26
S9	Calculated $E_a$ and approximate reversion rates . . . . .	S30
S10	<i>anti-trans</i> -OMe-PAI TDDFT excitations . . . . .	S31
S11	<i>anti-trans</i> -OMe-PAI-Ph TDDFT excitations . . . . .	S33

All xyz coordinates of optimized geometries are available to download at  
<https://github.com/fredingroup/azodyes/tree/main/indole>

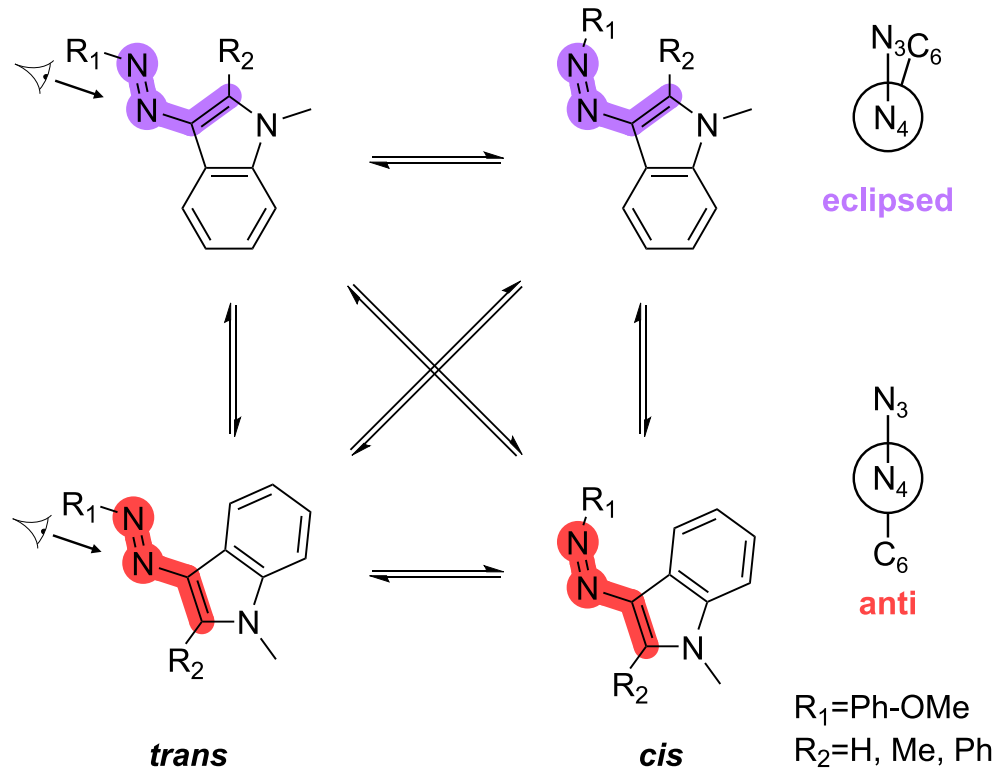


Fig. S1: Schematic representation of all the rotamers of OMe-PAI and OMe-PAI-Ph. *Trans* and *cis* are defined by the azo dihedral ( $D_{2345}$ , Table 1)), *eclipsed* and *anti* are defined by the indole dihedral ( $D_{3456}$ ),  $R_1 = \text{Ph-OMe}$  and  $R_2 = \text{H, Ph}$ .

## 1 Synthesis and Experimental Results

OMe-PAI and OMe-PAI-Ph were prepared by azo coupling in a similar manner to literature procedures.<sup>1,2</sup>

Fresh stock solutions of the azo molecules were prepared in dry acetonitrile (MeCN) at 0.3 mM

Table S1: Experimental photoisomerization and thermal reversion lifetimes of OMe-PAI and OMe-PAI-Ph determined through changes in absorbance spectra. Standard deviations are denoted in parentheses

	$\tau_{Isom}$ (msec)	$\tau_{Rev}$ (sec)
OMe-PAI	115.1 (4.1)	716 (85)
OMe-PAI-Ph	206 (18)	182 (41)

and diluted to a concentration of  $0.1 \mu\text{M}$  for spectral analysis. 2.00 mL of the dilute solution was transferred to a 1 cm quartz cuvette and placed in the sample holder of an OceanOptics Flame UV-vis spectrophotometer. Photoisomerization ( $trans \rightarrow cis$ ) was observed by monitoring the spectral change over time upon overhead illumination with a LuzChem LEDi-HUV7 lamp head ( $\lambda_{max} = 375 \text{ nm}$ ) and LuzChem LED Illuminator at 337 mW. After a photostationary state was reached, the illumination source was removed and spectra indicating thermal reversion ( $cis \rightarrow trans$ ) were collected. Isomerization and reversion lifetimes were determined by taking kinetic traces of the absorbance change at the maximum wavelength of the *trans* feature and fitting the data to a monoexponential decay model.

$^1\text{H}$  NMR were collected at  $-30^\circ\text{C}$  in deuterated DMF using a Bruker Avance NEO 500 MHz spectrometer with a Bruker SmartCooler BCU II prior to NOESY experiments. Data was collected using Topspin 4.4.0 and processed in MestReNova 6.0.2.

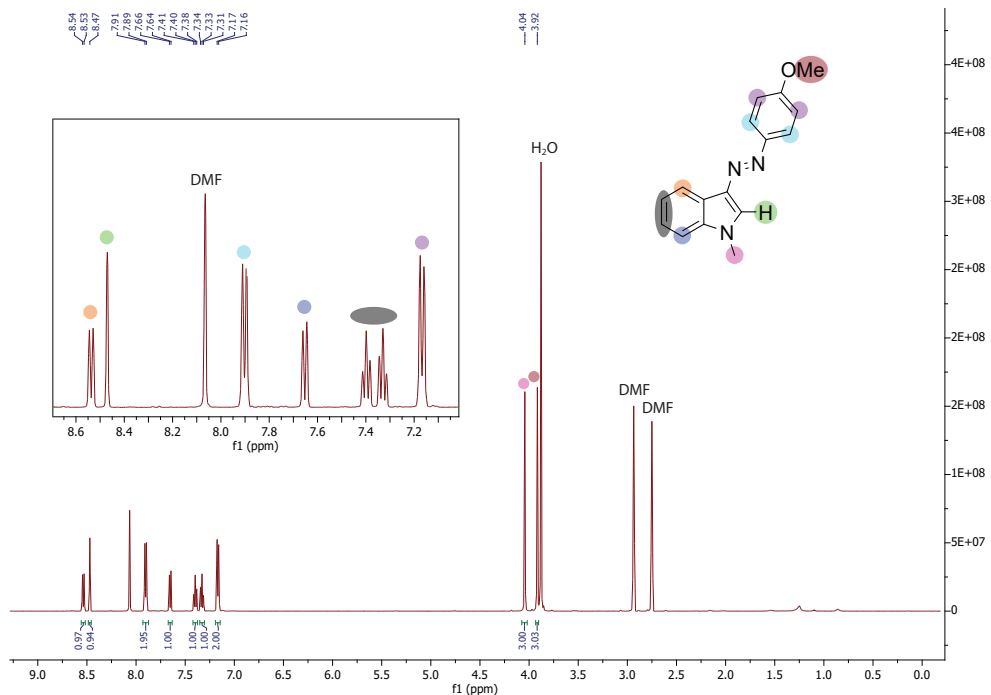


Fig. S2:  $^1\text{H}$  NMR of *trans*-OMe-PAI (500 MHz, DMF,  $-30^\circ\text{C}$ ).  $\delta$  8.54 (d,  $J = 7.8 \text{ Hz}$ , 1H), 8.47 (s, 1H), 7.90 (d,  $J = 7.7 \text{ Hz}$ , 2H), 7.65 (d,  $J = 8.1 \text{ Hz}$ , 1H), 7.40 (t,  $J = 7.6 \text{ Hz}$ , 1H), 7.33 (t,  $J = 7.5 \text{ Hz}$ , 1H), 7.17 (d,  $J = 7.7 \text{ Hz}$ , 2H), 4.04 (s, 3H), 3.92 (s, 3H)

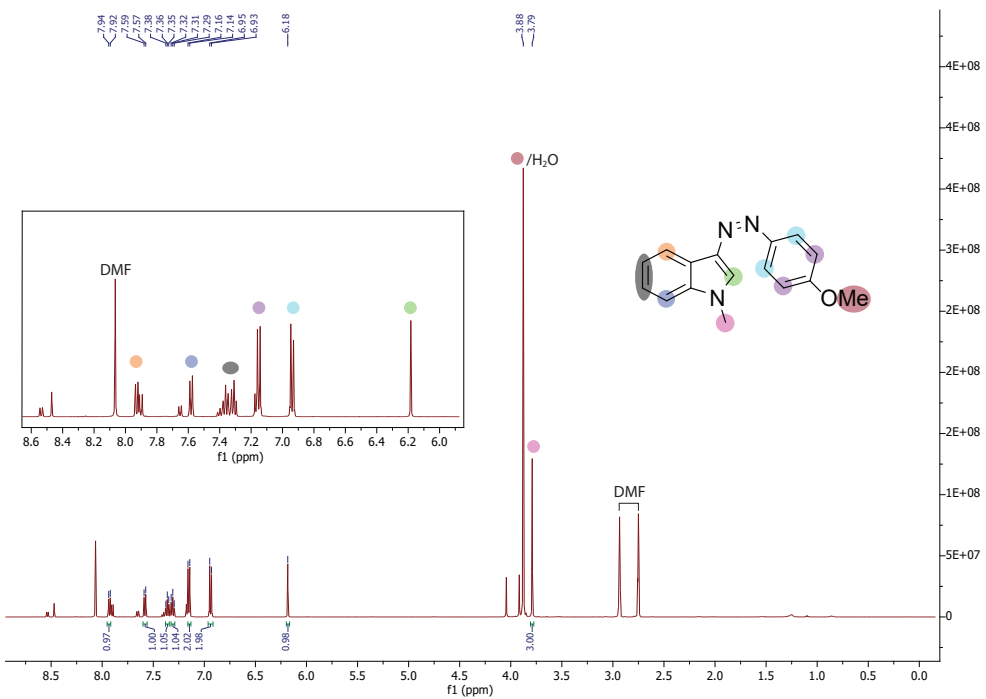


Fig. S3:  $^1\text{H}$  NMR of *cis*-OMe-PAI (500 MHz, DMF,  $-30^\circ\text{C}$ ).  $\delta$  7.93 (d,  $J = 7.8$  Hz, 1H), 7.58 (d,  $J = 8.1$  Hz, 1H), 7.36 (t,  $J = 7.1$  Hz, 1H), 7.31 (t,  $J = 7.5$  Hz, 1H), 7.15 (d,  $J = 8.7$  Hz, 2H), 6.94 (d,  $J = 8.8$  Hz, 2H), 6.18 (s, 1H), 3.88 (s, overlapped with  $\text{H}_2\text{O}$  at  $-30^\circ\text{C}$ ), 3.79 (s, 3H)

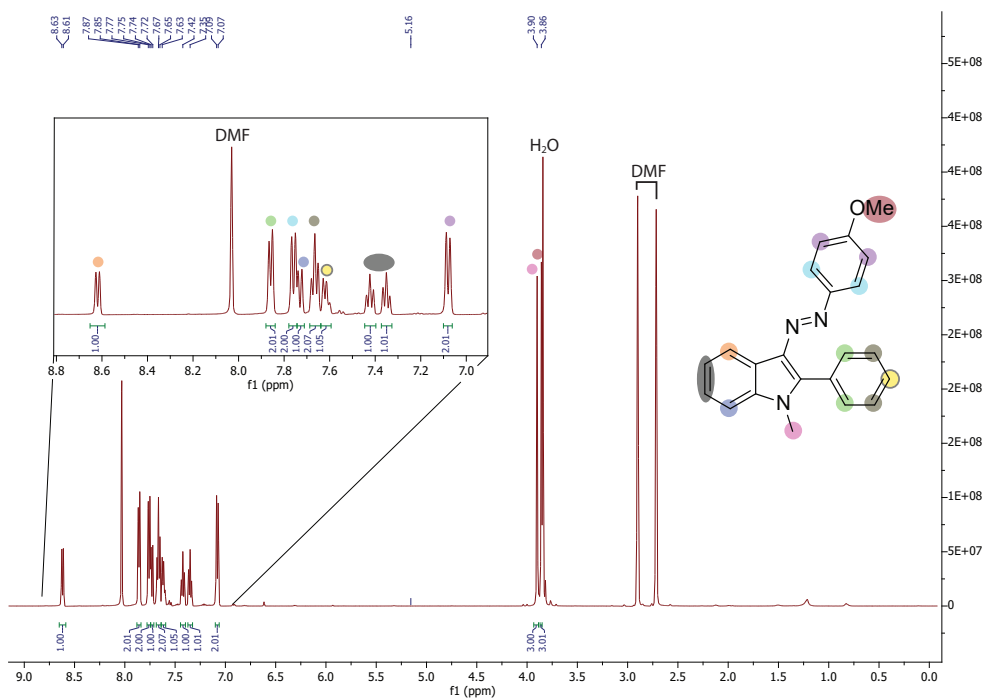


Fig. S4:  $^1\text{H}$  NMR of *trans*-OMe-PAI-Ph (500 MHz, DMF,  $-30^\circ\text{C}$ ).  $\delta$  8.62 (d,  $J = 7.8 \text{ Hz}$ , 1H), 7.86 (d,  $J = 7.4 \text{ Hz}$ , 2H), 7.76 (d,  $J = 7.9 \text{ Hz}$ , 2H), 7.73 (d,  $J = 8.4 \text{ Hz}$ , 1H), 7.67 (t,  $J = 7.3 \text{ Hz}$ , 2H), 7.62 (d,  $J = 6.8 \text{ Hz}$ , 1H), 7.42 (t,  $J = 7.6 \text{ Hz}$ , 1H), 7.35 (t,  $J = 7.4 \text{ Hz}$ , 1H), 7.08 (d,  $J = 7.9 \text{ Hz}$ , 2H), 3.90 (s, 3H), 3.86 (s, 3H)

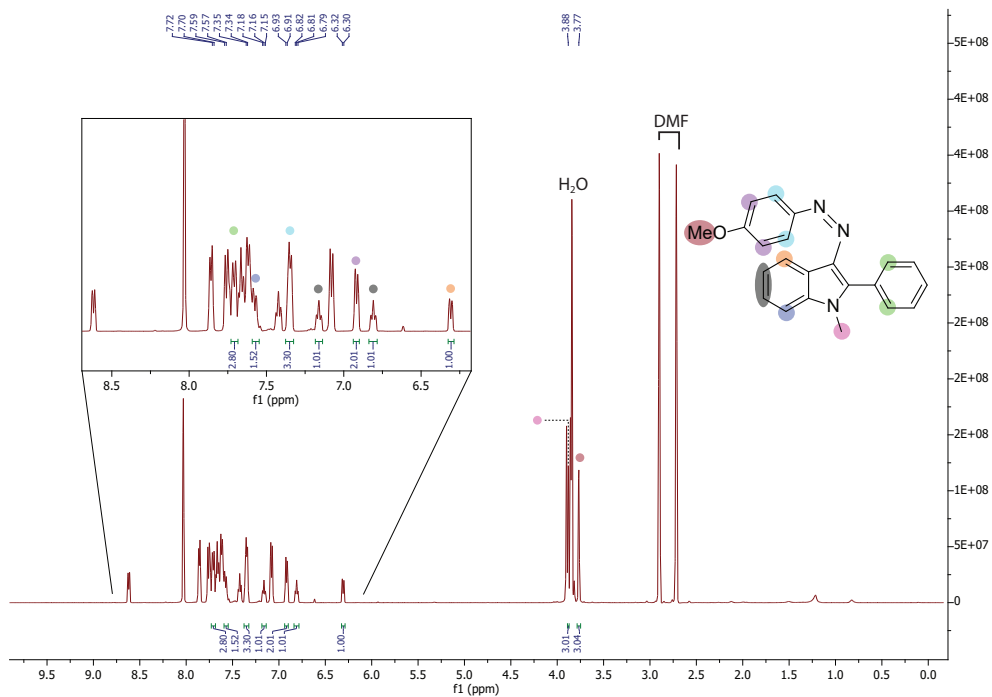


Fig. S5:  $^1\text{H}$  NMR of *cis*-OMe-PAI-Ph (500 MHz, DMF,  $-30^\circ\text{C}$ ).  $\delta$  7.71 (d,  $J = 9.2 \text{ Hz}$ , 2H), 7.58 (d,  $J = 9.1 \text{ Hz}$ , 1H), 7.35 (d,  $J = 7.5 \text{ Hz}$ , 2H), 7.16 (t,  $J = 7.4 \text{ Hz}$ , 1H), 6.92 (d,  $J = 7.8 \text{ Hz}$ , 2H), 6.81 (t,  $J = 7.3 \text{ Hz}$ , 1H), 6.31 (d,  $J = 7.9 \text{ Hz}$ , 1H), 3.88 (s, 3H), 3.77 (s, 3H)

**NOESY Sample Prep:** Samples were prepared by dissolving the solid dye in 1 mL of deuterated DMF to create a 10 mM solution. This solution was then passed through a 0.22 micron nylon filter into a Norell S500 7" valved VT NMR tube that had been previously washed with acetone and dried in the oven overnight. The sample was freeze-pump-thawed on a Schlenk line and brought to a pressure of 6-10 torr. The spectrometer temperature was lowered to -30°C to slow the thermal reversion rate of the *cis* isomer over the course of the experiment.

**NOESY Instrumental Information:**  $^1\text{H}$ - $^1\text{H}$  NOESY experiments were performed on a Bruker Avance NEO 500 MHz spectrometer with a Bruker SmartCooler BCU II to decrease the temperature. Data was collected using TopSpin 4.4.0 with the noesygpph pulse sequence (NS = 4, D[8] = 0.7 sec). The resulting spectra were processed by manual phase correction of the rows and columns and phase-sensitive symmetrization (syma) to reduce noise.

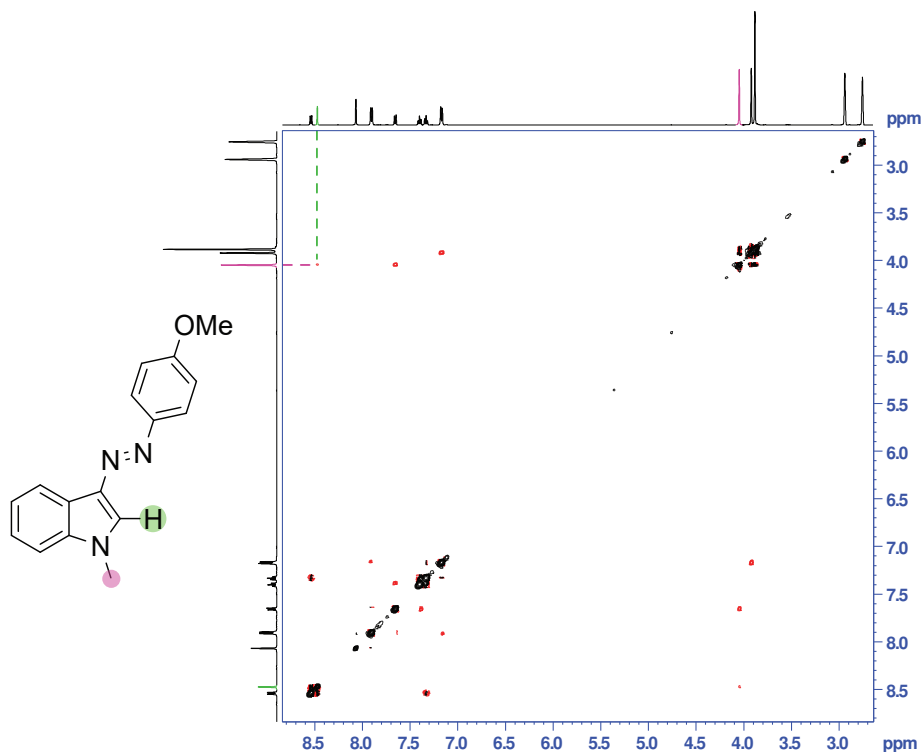


Fig. S6:  $^1\text{H}$ - $^1\text{H}$  NOESY of *trans*-OMe-PAI (500 MHz, DMF, -30°C).

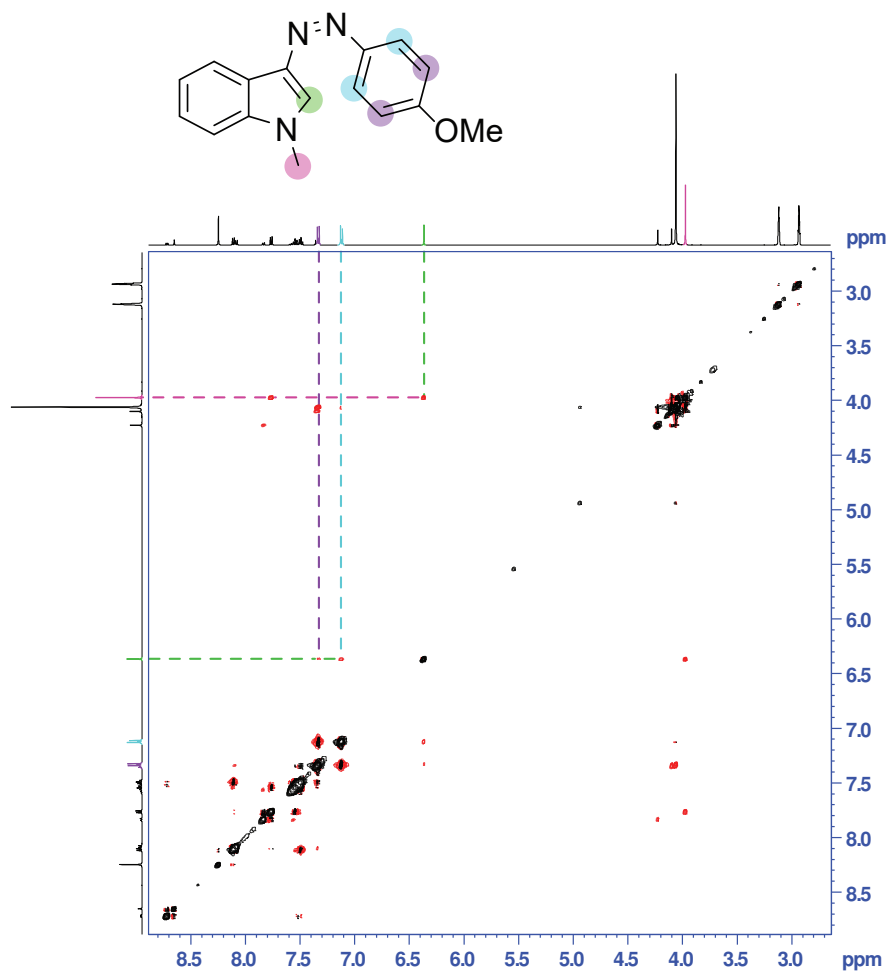


Fig. S7:  $^1\text{H}$ - $^1\text{H}$  NOESY of *cis*-OMe-PAI (500 MHz, DMF, -30°C). The signals denoted by the crossing of the green and purple/light blue lines indicates interspatial interactions between the substituent proton and the protons of the p-methoxyphenyl ring.

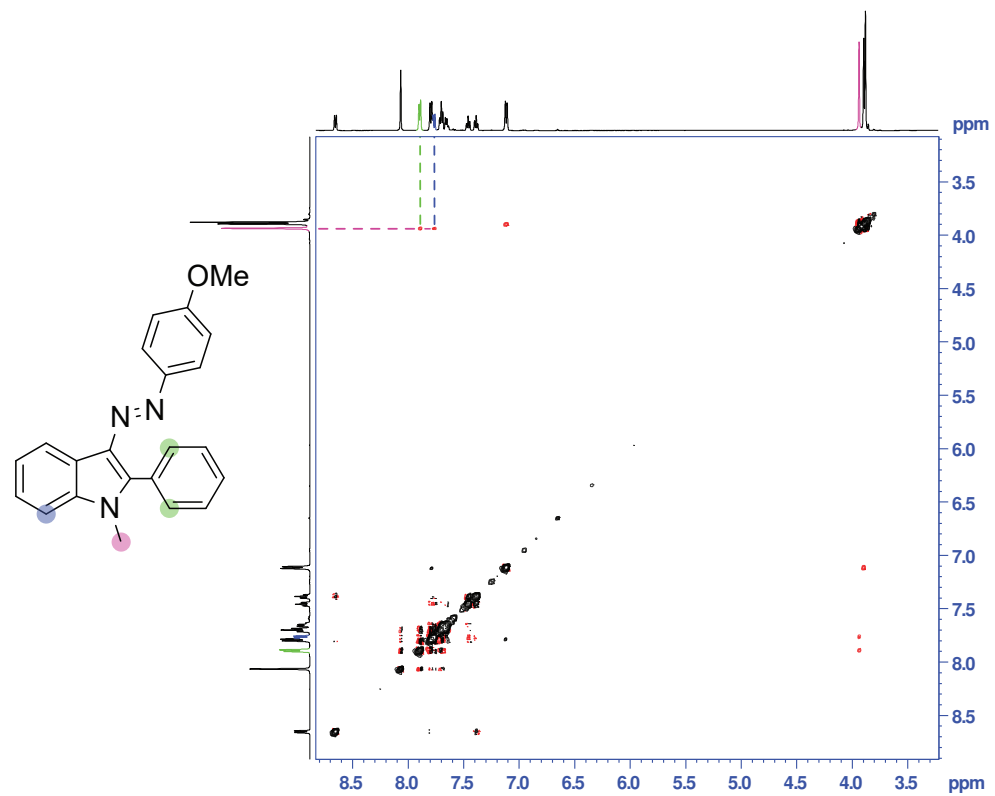


Fig. S8:  $^1\text{H}$ - $^1\text{H}$  NOESY of *trans*-OMe-PAI-Ph (500 MHz, DMF, -30°C).

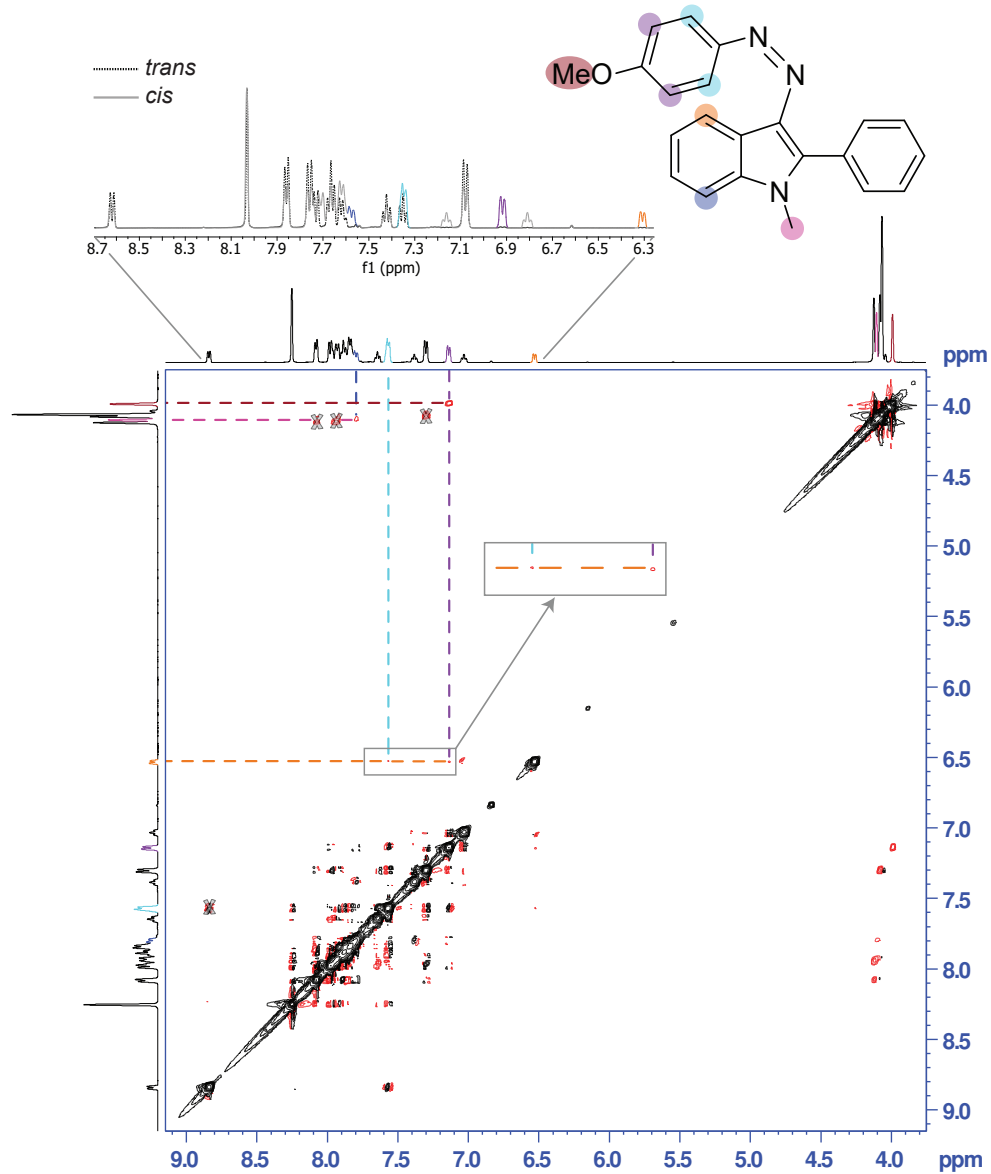


Fig. S9:  $^1\text{H}$ - $^1\text{H}$  NOESY of *cis*-OMe-PAI-Ph (500 MHz, DMF, -30°C). The signals denoted by the crossing of the orange and purple/light blue lines indicate interspatial interactions between the indole doublet closest to the azo bond with the protons of the p-methoxyphenyl ring. The maroon and purple lines indicate the interaction between the -OMe singlet and the closest doublet of the p-methoxyphenyl ring. The pink and dark blue lines indicate the interaction between the -NMe singlet and the indole doublet furthest from the azo bond. Light grey X's indicate interactions arising from trans isomer present in the sample during time of analysis.

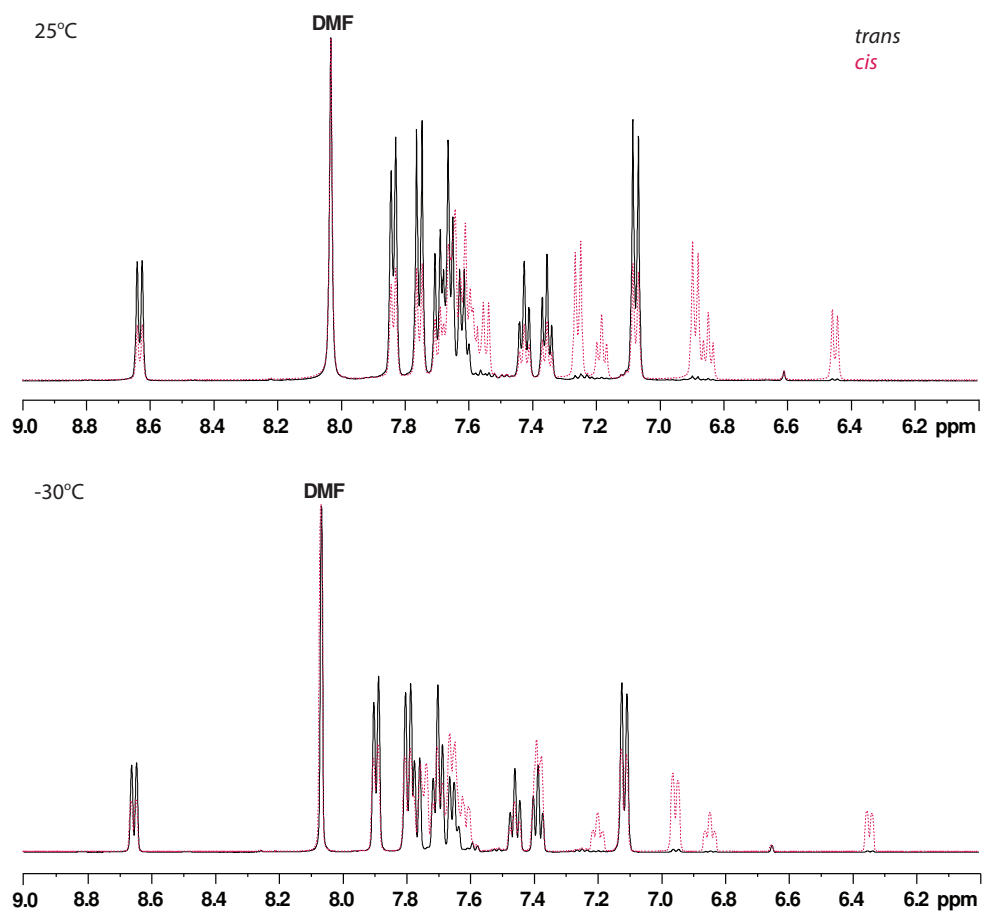


Fig. S10: Room temperature (25°C) and -30°C NMR of OMe-PAI-Ph (500 MHz, DMF).

## 2 Quantum Mechanical Calculations

Phenyl-azo-indoles (PAIs) in all possible rotameric states were optimized at CAM-B3LYP-D3BJ/6-311G(d,p)/PCM(MeCN) level of theory in Gaussian 16<sup>3</sup> and confirmed as true minima without imaginary frequencies. Ground-state ( $S_0$ ) potential energy curves (PECs) were optimized with the marked coordinate frozen (Figure 2). Starting from the lowest energy *trans*-isomer (Table S2), each degree of freedom of the azo bond including the CNNC rotation and the  $^{Ind}CNN$  and  $^{Ph}CNN$  inversions were scanned toward the corresponding *cis*-isomer. Nonconverged geometries near the conical intersections were removed to provide the most realistic PESs. On each multidimensional potential energy surface (PES), each marked point on  $S_0$  is a constrained optimization where only the CNNC dihedral angle and the respective CNN angle were frozen. The excited-state energies of  $S_1$  and  $S_2$  were calculated as *single-point energies* using time-dependent density functional theory (TD-DFT).

### 2.1 Optimized Structures

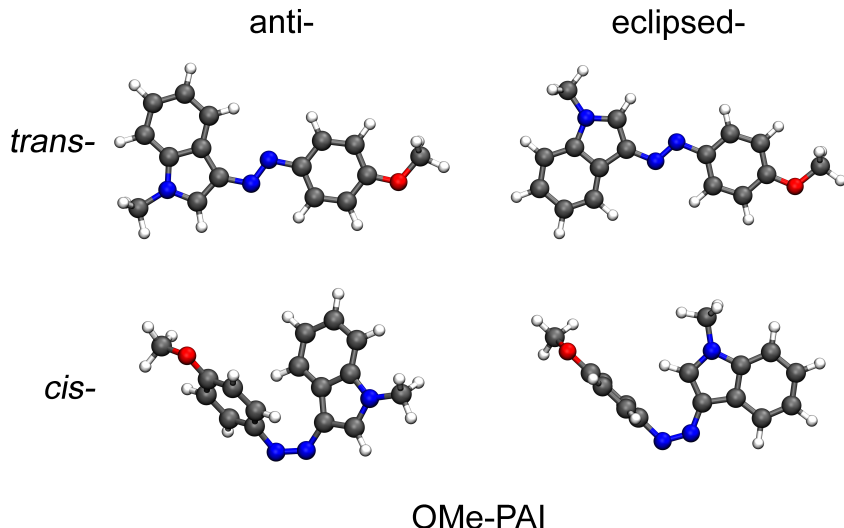


Fig. S11: Four optimized meta-stable rotamers of OMe-PAI at CAM-B3LYP/6-311G(d,p)-D3BJ/PCM(MeCN) level of theory.

Table S2: *Trans*-isomer and *cis*-isomer energies (eV) for OMe-PAI and OMe-PAI-Ph at CAM-B3LYP/6-311G(d,p)-D3BJ/PCM(MeCN) level of theory. Boltzmann weights at 300 K are in parentheses.

	<i>anti-trans</i> (eV)	<i>eclipsed-trans</i> (eV)	<i>anti-cis</i> (eV)	<i>eclipsed-cis</i> (eV)
OMe-PAI	0.000 (96.1%)	0.083 (3.9%)	0.604 (21.4%)	0.570 (78.6%)
OMe-PAI-Ph	0.000 (99.9%)	0.171 (0.1%)	0.646 (3.6%)	0.561 (96.4%)

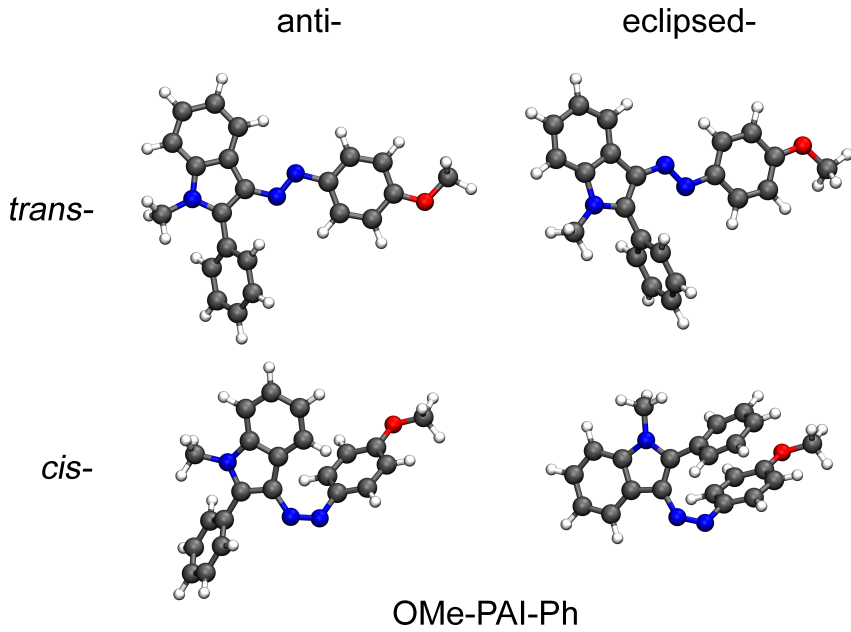


Fig. S12: Four optimized meta-stable rotamers of OMe-PAI-Ph at CAM-B3LYP/6-311G(d,p)-D3BJ/PCM(MeCN) level of theory.

Table S3: DLPNO-CCSD(T)/cc-pVTZ/SMD(MeCN) energies of CAM-B3LYP-D3(BJ)/6-311g(d,p)/PCM(MeCN) optimized structures. E(HF) are the SCF Hartree-Fock energies. E(0) are the solvent corrected reference energies for DLPNO-CCSD(T). E(CCSD) are the CCSD energies and E(CCSD(T)) are the CCSD(T) energies. The lowest energies for each isomer and solvent are highlighted yellow.

	<i>anti-cis</i> -OMe-PAI (MeCN)	<i>eclipsed-cis</i> -OMe-PAI (MeCN)	<i>anti-cis</i> -OMe-PAI-Ph (MeCN)	<i>eclipsed-cis</i> -OMe-PAI-Ph (MeCN)
E(HF) (Ha)	-853.049451393	-853.053479428	-1082.669261286	-1082.665633934
E(0)=E(HF)+G <sub>cds</sub> (Ha)	-853.052186568	-853.056700063	-1082.674694411	-1082.670715765
E(CCSD) (Ha)	-856.470866761	-856.473162636	-1087.042813728	-1087.044590546
E(CCSD(T)) (Ha)	-856.644652615	-856.646363122	-1087.268393056	-1087.270943738

Table S4: DLPNO-CCSD(T)/cc-pVTZ/SMD(DMF) energies of CAM-B3LYP-D3(BJ)/6-311g(d,p)/PCM(DMF) optimized structures. E(HF) are the SCF Hartree-Fock energies. E(0) are the solvent corrected reference energies for DLPNO-CCSD(T). E(CCSD) are the CCSD energies and E(CCSD(T)) are the CCSD(T) energies. The lowest energies for each isomer and solvent are highlighted yellow.

	<i>anti-cis</i> -OMe-PAI-Ph (DMF)	<i>eclipsed-cis</i> -OMe-PAI-Ph (DMF)
E(HF) (Ha)	-1082.669096335	-1082.665454823
E(0)=E(HF)+G <sub>cds</sub> (Ha)	-1082.671561082	-1082.667859953
E(CCSD) (Ha)	-1087.039699433	-1087.041752002
E(CCSD(T)) (Ha)	-1087.265285926	-1087.268112934

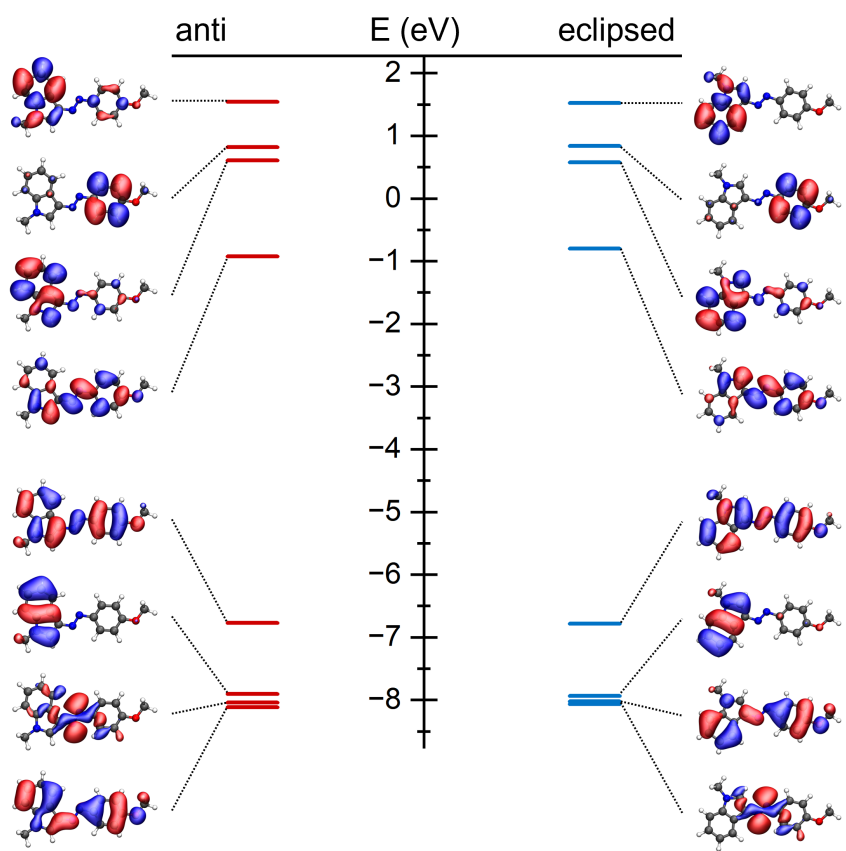


Fig. S13: Molecular orbitals of the optimized *trans*-rotamers of OMe-PAI at CAM-B3LYP/6-311G(d,p)-D3BJ/PCM(MeCN) level of theory.

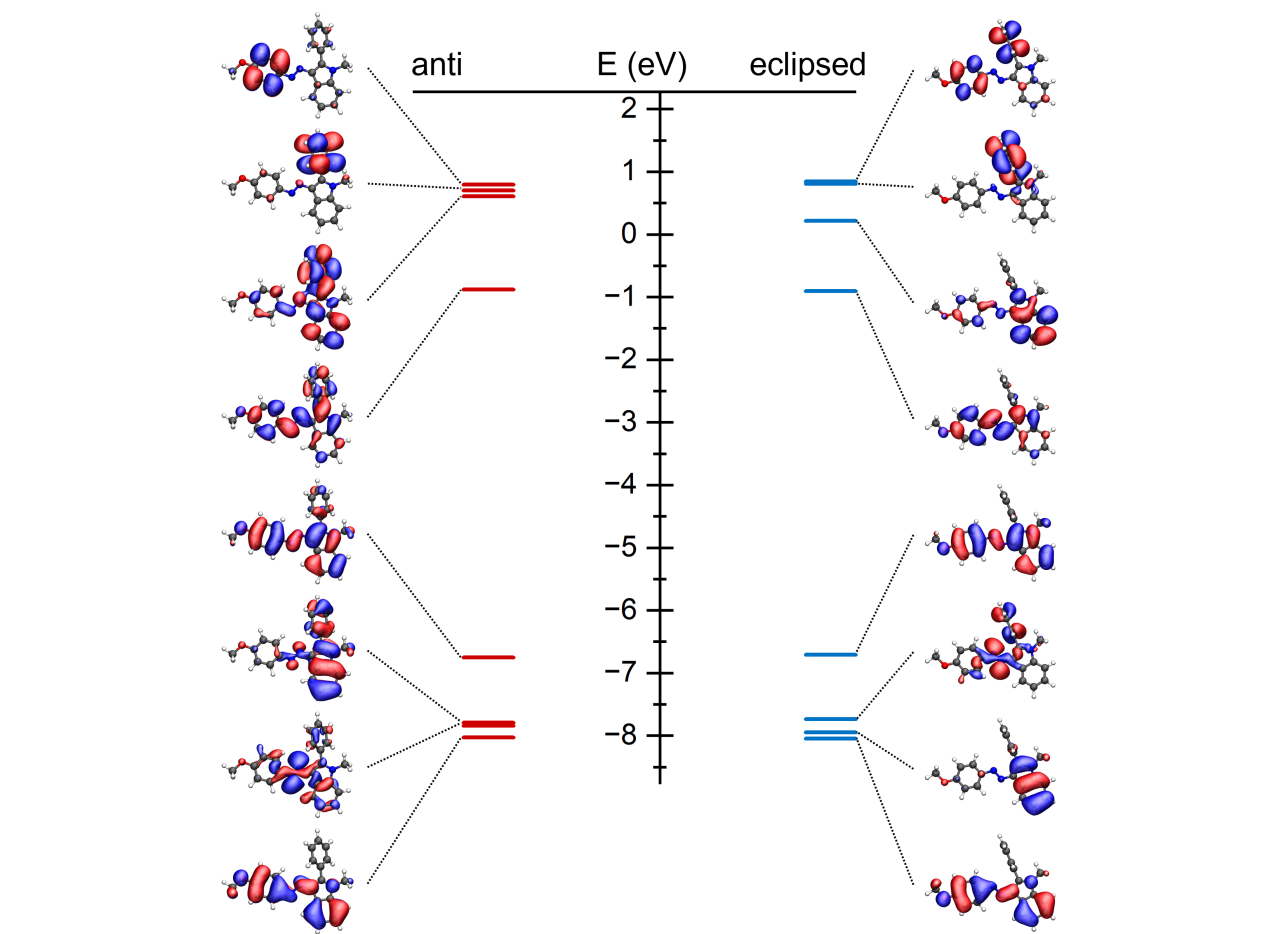


Fig. S14: Molecular orbitals of the optimized *trans*-rotamers of OMe-PAI-Ph at CAM-B3LYP/6-311G(d,p)-D3BJ/PCM(MeCN) level of theory.

## 2.2 Transition States with Displacement Vectors

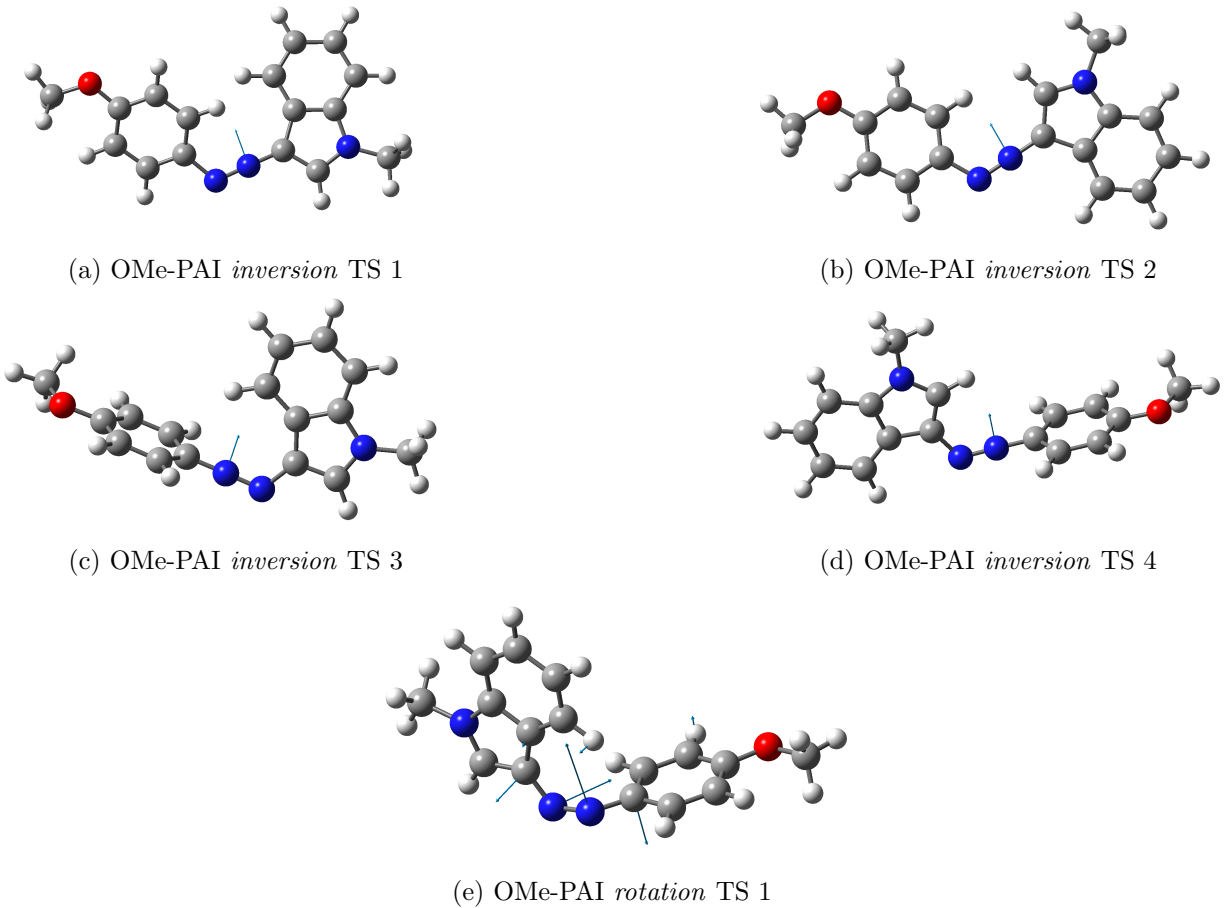


Fig. S15: OMe-PAI *trans*→*cis* transition state structures with displacement vectors optimized at CAM-B3LYP/6-311G(d,p)-D3BJ/PCM(MeCN) level of theory and confirmed as true transition state with a single imaginary frequency mode.

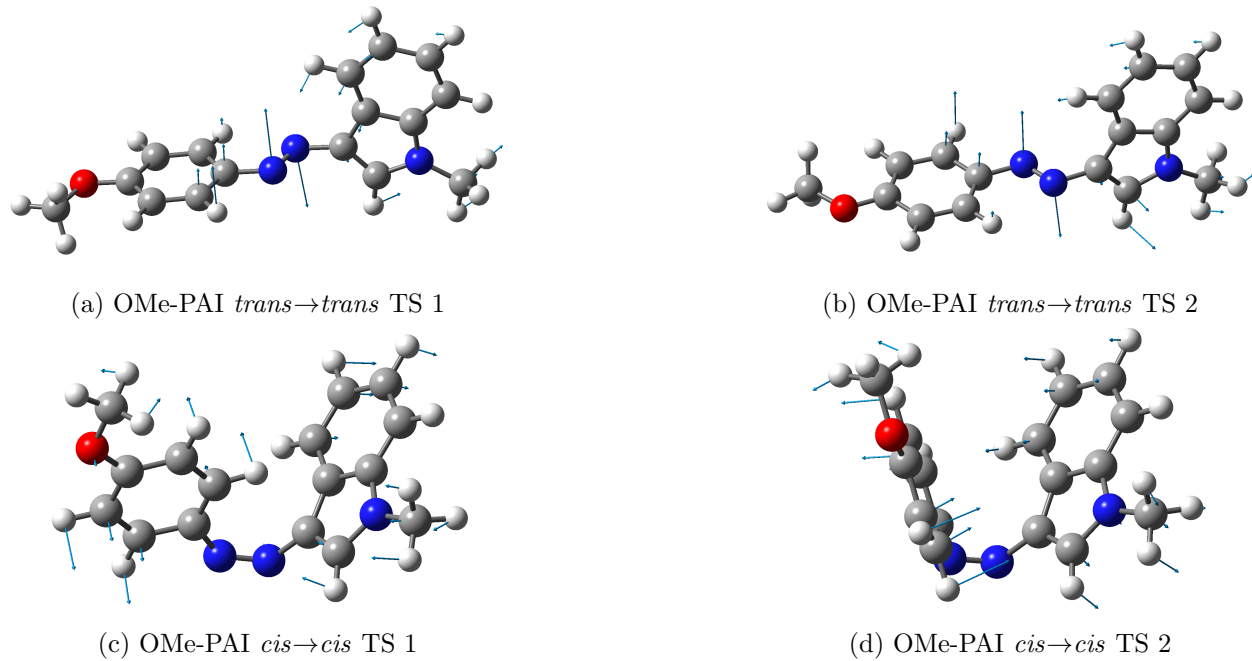


Fig. S16: OMe-PAI *trans*→*trans* and *cis*→*cis* transition state structures with displacement vectors optimized at CAM-B3LYP/6-311G(d,p)-D3BJ/PCM(MeCN) level of theory and confirmed as true transition state with one imaginary frequency.

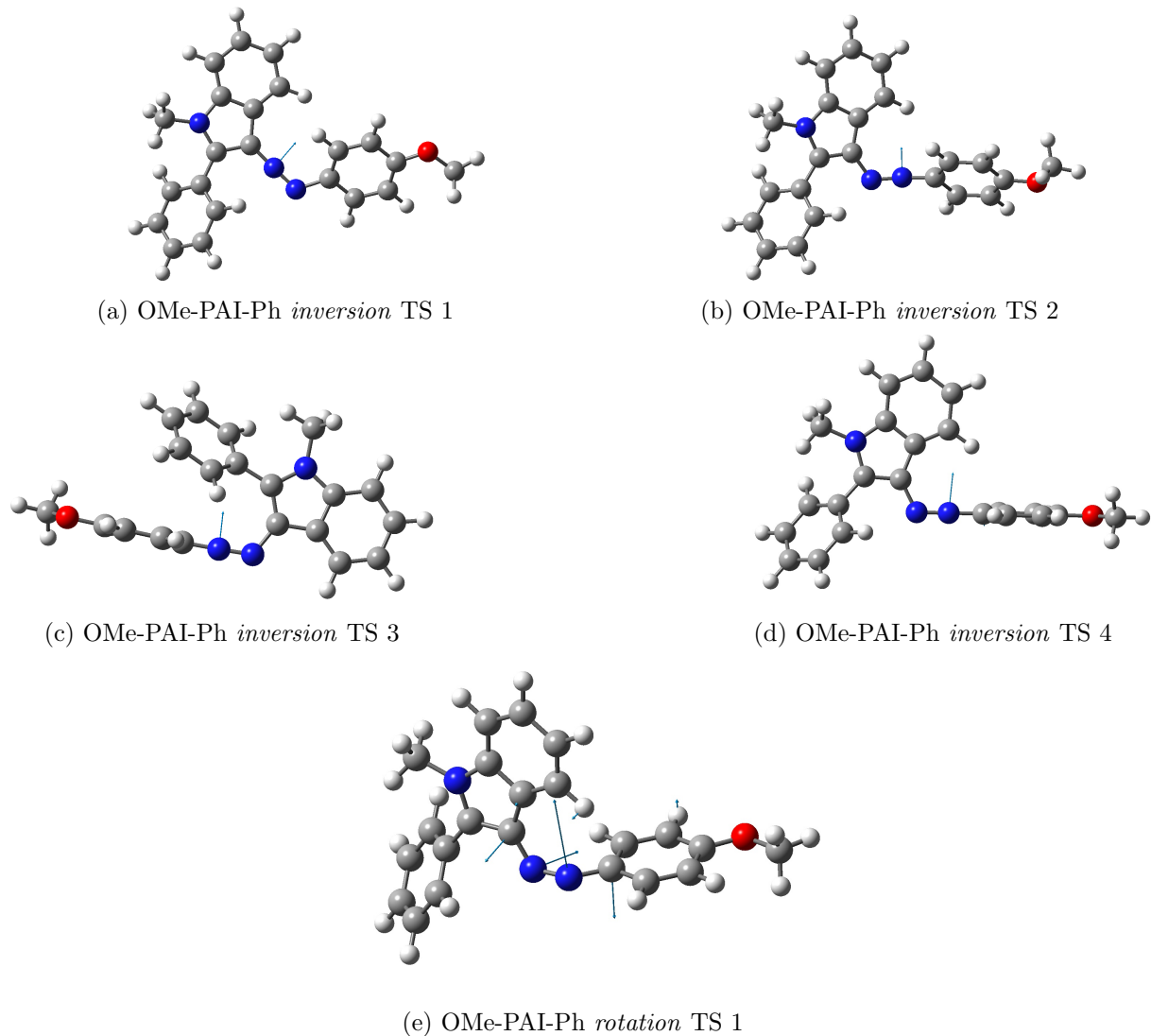
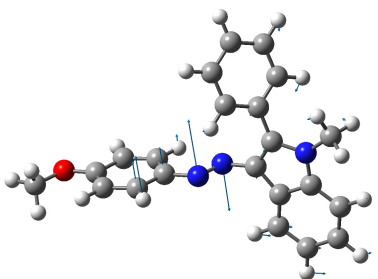
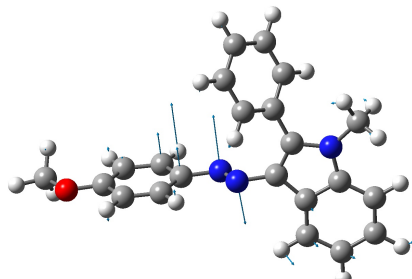


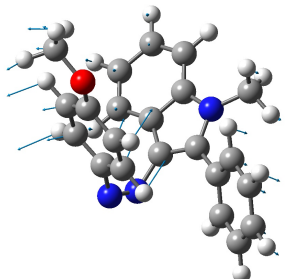
Fig. S17: OMe-PAI-Ph *trans*→*cis* transition state structures with displacement vectors, found at CAM-B3LYP/6-311G(d,p)-D3BJ/PCM(MeCN) level of theory and confirmed as true transition states with one imaginary frequency.



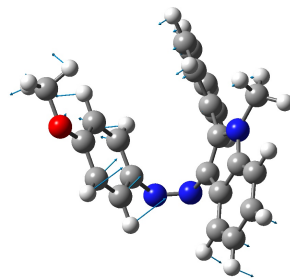
(a) OMe-PAI-Ph *trans*→*trans* TS 1



(b) OMe-PAI-Ph *trans*→*trans* TS 2



(c) OMe-PAI-Ph *cis*→*cis* TS 1



(d) OMe-PAI-Ph *cis*→*cis* TS 2

Fig. S18: OMe-PAI-Ph *trans*→*trans* or *cis*→*cis* transition state structures with displacement vectors optimized at CAM-B3LYP/6-311G(d,p)-D3BJ/PCM(MeCN) level of theory and confirmed as true transition state with one imaginary frequency.

### 2.3 Method Comparison for Excited State Scan Calculations

In order to verify the *point excitation* method presented in the main text, we used a few different methods to calculate the excited-state surfaces. Overall, calculating the excited state energies without structural optimization greatly reduces the computation time without a significant loss in the reliability to describe the isomerization mechanisms.

*Point excitation* is commonly used to construct a picture of the excited state surfaces (in particular those with the same spin) above a ground state surface. This approximation assumes that the ground-state geometry is representative of the excited-state nuclear coordinates with only the electronic structure varying. Alternatively, particular excited states (*e.g.*  $S_1$  or  $S_2$ ) could be re-optimized at each constrained geometry, providing a TD-DFT *optimized point excitation*. Finally, the excited state surface could be explored from the initially excited Franck-Condon geometry using a TD-DFT *excited scan*. PECs calculated using these different methods are compared in Figure S19.

For  $S_1$ , the *point excitation* (green-triangle) energies minimally deviate from the optimized energies, either *optimized point excitations* (orange-triangle) or *excited scan* (purple-triangle). The energy deviation of  $S_1$  starts at about 0.5 eV for *anti-trans*-OMe-PAI (CNNC dihedral  $\approx 180^\circ$ ) and slowly decreases to about 0.2 eV near the conical intersection.

For  $S_2$ , the *point excitation* (yellow-diamond) energies deviate from the optimized energies by about 0.5 eV at CNNC dihedral  $\approx 180^\circ$ , and then increase to 0.9 eV at CNNC dihedral  $\approx 100^\circ$ . For both  $S_1$  and  $S_2$  *point excitations* provide similar insights into the photoisomerization mechanism at a much lower computational cost. Using the same compute node, the *point excitation* method is about 35 times faster than the *optimized point excitation* method and about 54 times faster than *excited scan*.

The *optimized point excitation* and *excited scan* calculations are unstable along  $S_2$  reaction coordinate. For both optimization methods, relaxation from the  $S_2$  to  $S_1$  (Figure S19). This poses a major issue for azo dyes because the  $S_1$  and  $S_2$  excited state are of different character (*i.e.*  $S_1$  is  $n \rightarrow \pi^*$  and  $S_2$  is  $\pi \rightarrow \pi^*$ ). The *optimized point excitation* switches back and forth between the  $S_2$  state and the optimized lower energy  $S_1$  state for different geometries. For the *optimized scan*, intermediate points did not fully converge, making most of their energies unusable.

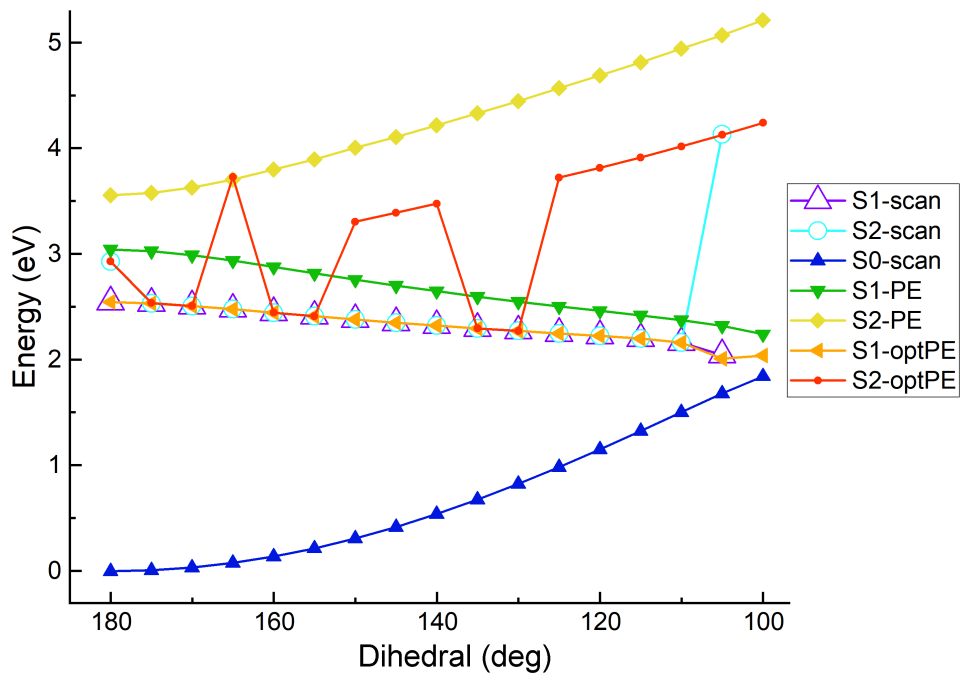


Fig. S19: Method comparison for excited state PEC calculations at CAM-B3LYP/6-311G(d,p)-D3BJ/PCM(MeCN) level of theory, demonstrated by rotation scan from CNNC  $\approx 180^\circ$  of *anti-trans*-OMe-PAI. *Point excitation* (PE) is the direct TD excitation of ground state geometries extracted from  $S_0$  PEC (blue-triangle). *Optimized point excitation* (optPE) TD optimizes the  $S_n$  excited state with dihedral angle fixed at that point. *Optimized scan* (scan) is a relaxed TD  $S_n$  scan of the dihedral rotation starting at excited *anti-trans*-OMe-PAI geometry.

## 2.4 Potential Energy Surfaces

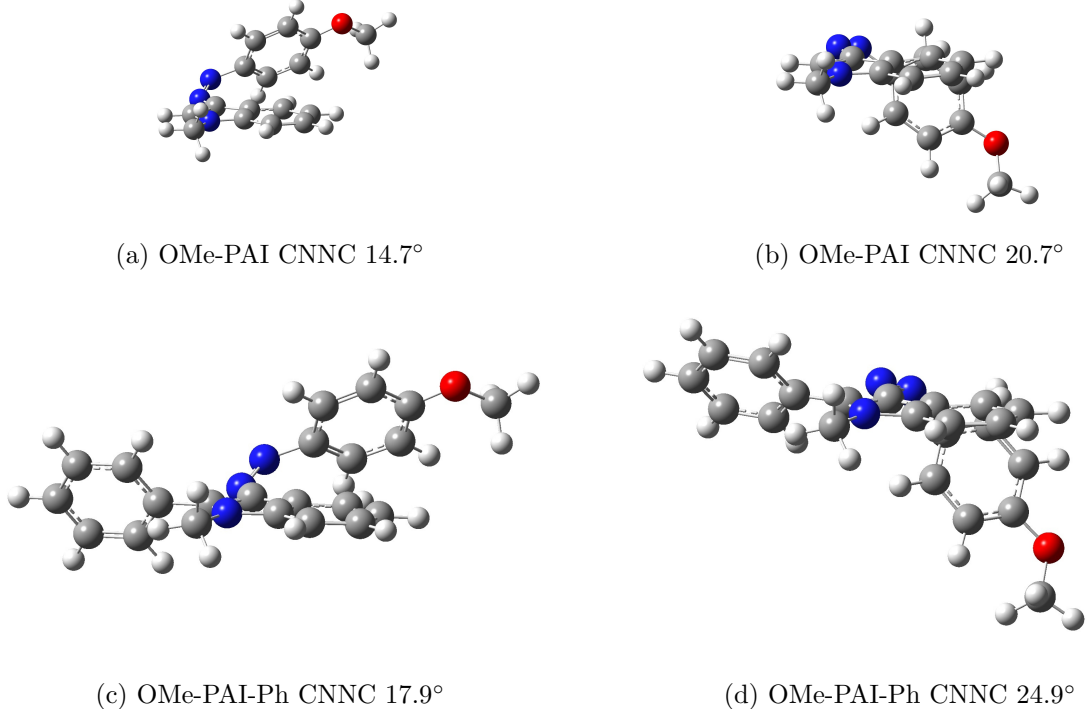


Fig. S20: Computed geometries OMe-PAI (top) and OMe-PAI-Ph (bottom)  $S_0$  PECs (Figure 2) on either side of the discontinuities around CNNC 20° (right). Each point along the  $S_0$  was optimized with only the CNNC dihedral frozen and the lowest energy structure obtained at each point are used to construct the PECs. CAM-B3LYP/6-311G(d,p)-D3BJ/PCM(MeCN).

Table S5: Computed energies on the  $S_0$   $^{Ind}$ CNN OMe-PAI PES. CAM-B3LYP/6-311G(d,p)-D3BJ/PCM(MeCN).

Dihedral (deg)	Angle (deg)	Energy (eV)
180	115	0.000
155	115	0.217
130	115	0.827
105	115	1.683
80	115	1.832
55	115	1.203
30	115	0.811
5	115	0.727
180	125	0.129
164	125	0.214
148	125	0.463
132	125	0.859
116	125	1.371
100	125	1.941
84	125	1.923

68	125	1.463
52	125	1.058
36	125	0.776
20	125	0.627
4	125	0.607
180	135	0.454
164	135	0.531
148	135	0.755
132	135	1.111
116	135	1.575
100	135	2.107
84	135	2.051
68	135	1.577
52	135	1.184
36	135	0.901
20	135	0.740
4	135	0.705
180	145	0.882
155	145	1.033
130	145	1.454
105	145	2.016
80	145	2.048
55	145	1.525
30	145	1.152
5	145	1.022
180	155	1.316
155	155	1.417
130	155	1.684
105	155	1.977
80	155	1.981
55	155	1.702
30	155	1.457
5	155	1.367
180	165	1.664
155	165	1.707
130	165	1.813
105	165	1.909
80	165	1.907
55	165	1.813
30	165	1.712
5	165	1.672
180	175	1.849
155	175	1.853
130	175	1.862
105	175	1.870
80	175	1.869
55	175	1.862
30	175	1.852

5	175	1.848
---	-----	-------

Table S6: Computed energies on the  $S_0$   $^{Ph}$ CNN OMe-PAI PES. CAM-B3LYP/6-311G(d,p)-D3BJ/PCM(MeCN).

Dihedral (deg)	Angle (deg)	Energy (eV)
180	115	0.000
155	115	0.217
130	115	0.828
105	115	1.692
80	115	1.887
55	115	1.197
30	115	0.796
5	115	0.703
180	125	0.145
155	125	0.345
130	125	0.915
105	125	1.707
80	125	1.797
55	125	1.128
30	125	0.710
5	125	0.608
180	135	0.510
155	135	0.677
130	135	1.162
105	135	1.789
80	135	1.819
55	135	1.260
30	135	0.866
5	135	0.764
180	145	0.998
155	145	1.097
130	145	1.449
105	145	1.854
80	145	1.859
55	145	1.478
30	145	1.166
5	145	1.078
174	155	1.431
161	155	1.453
136	155	1.626
111	155	1.846
86	155	1.904
61	155	1.730
36	155	1.521
11	155	1.424
178	165	1.726

153	165	1.757
128	165	1.832
103	165	1.894
78	165	1.882
53	165	1.805
28	165	1.728
3	165	1.697
179	175	1.873
154	175	1.877
129	175	1.884
104	175	1.889
79	175	1.887
54	175	1.877
29	175	1.866
4	175	1.860

Table S7: Computed energies on the  $S_0$   $^{Ind}$ CNN OMe-PAI-Ph PES. CAM-B3LYP/6-311G(d,p)-D3BJ/PCM(MeCN).

Dihedral (deg)	Angle (deg)	Energy (eV)
180	115	0
160	115	0.12747
141	115	0.50306
121	115	1.07703
102	115	1.74215
82	115	1.86741
63	115	1.39098
43	115	0.98442
24	115	0.76287
4	115	0.72905
180	125	0.12299
164	125	0.20532
148	125	0.44678
132	125	0.83115
116	125	1.32677
100	125	1.88128
84	125	1.90817
68	125	1.46696
52	125	1.07675
36	125	0.80543
20	125	0.66465
4	125	0.65052
179	135	0.43223
160	135	0.54454
140	135	0.8677
121	135	1.35887
101	135	1.953

82	135	1.98211
62	135	1.44351
43	135	1.04036
23	135	0.80709
4	135	0.75767
178	145	0.84034
159	145	0.93319
139	145	1.19554
120	145	1.57773
100	145	1.97031
81	145	2.0926
61	145	1.82086
42	145	1.42649
22	145	1.13884
3	145	0.9936
177	155	1.25673
157	155	1.31847
138	155	1.48624
118	155	1.71167
99	155	1.90407
79	155	1.94594
60	155	1.80567
40	155	1.57583
21	155	1.38529
1	155	1.28649
175	165	1.58889
156	165	1.61576
136	165	1.68447
117	165	1.76691
97	165	1.82657
78	165	1.83315
58	165	1.78171
39	165	1.69546
19	165	1.61637
0	165	1.57485
174	175	1.76003
155	175	1.76228
135	175	1.76799
116	175	1.77436
96	175	1.77829
77	175	1.77767
57	175	1.77228
38	175	1.7639
18	175	1.75591
-1	175	1.75155

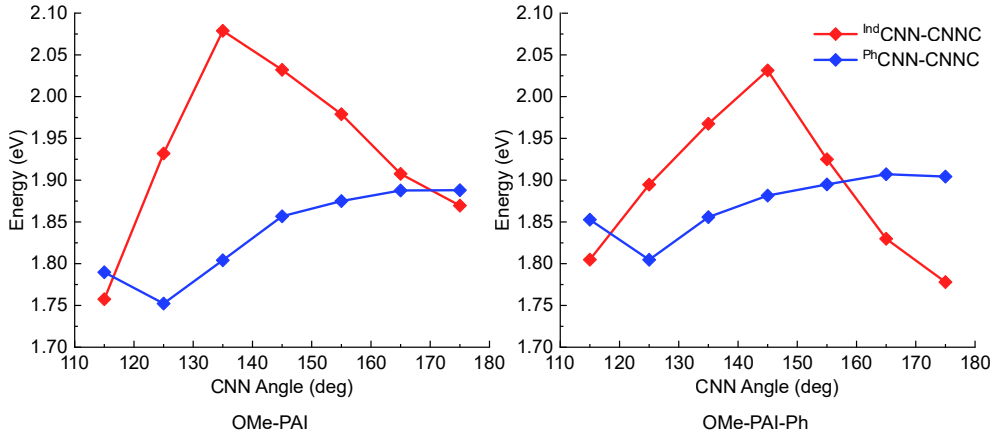


Fig. S21: Energies on PES, at  $\text{CNNC} \approx 90^\circ$ , obtained by average two closest data points near the  $90^\circ$  line.

Table S8: Computed energies on the  $S_0$   ${}^{Ph}\text{CNN}$  OMe-PAI-Ph PES. CAM-B3LYP/6-311G(d,p)-D3BJ/PCM(MeCN).

Dihedral (deg)	Angle (deg)	Energy (eV)
180	115	0.000
160	115	0.127
141	115	0.503
121	115	1.076
102	115	1.749
82	115	1.936
63	115	1.404
43	115	1.002
24	115	0.791
4	115	0.759
179	125	0.146
160	125	0.267
140	125	0.621
121	125	1.163
101	125	1.773
82	125	1.837
62	125	1.323
43	125	0.912
23	125	0.686
4	125	0.652
179	135	0.509
160	135	0.612
140	135	0.916
121	135	1.375
101	135	1.840
82	135	1.849
62	135	1.432

43	135	1.055
23	135	0.834
4	135	0.797
176	145	0.989
157	145	1.077
137	145	1.322
118	145	1.655
98	145	1.911
79	145	1.852
59	145	1.563
40	145	1.288
20	145	1.126
1	145	1.116
174	155	1.436
154	155	1.492
135	155	1.639
115	155	1.817
96	155	1.922
76	155	1.875
57	155	1.720
37	155	1.562
18	155	1.468
-2	155	1.439
177	165	1.732
163	165	1.747
144	165	1.792
124	165	1.855
105	165	1.904
85	165	1.910
66	165	1.869
46	165	1.804
27	165	1.747
7	165	1.716
179	175	1.885
162	175	1.887
142	175	1.893
123	175	1.900
103	175	1.905
84	175	1.904
64	175	1.898
45	175	1.889
25	175	1.880
6	175	1.875
18	175	1.75591
-1	175	1.75155

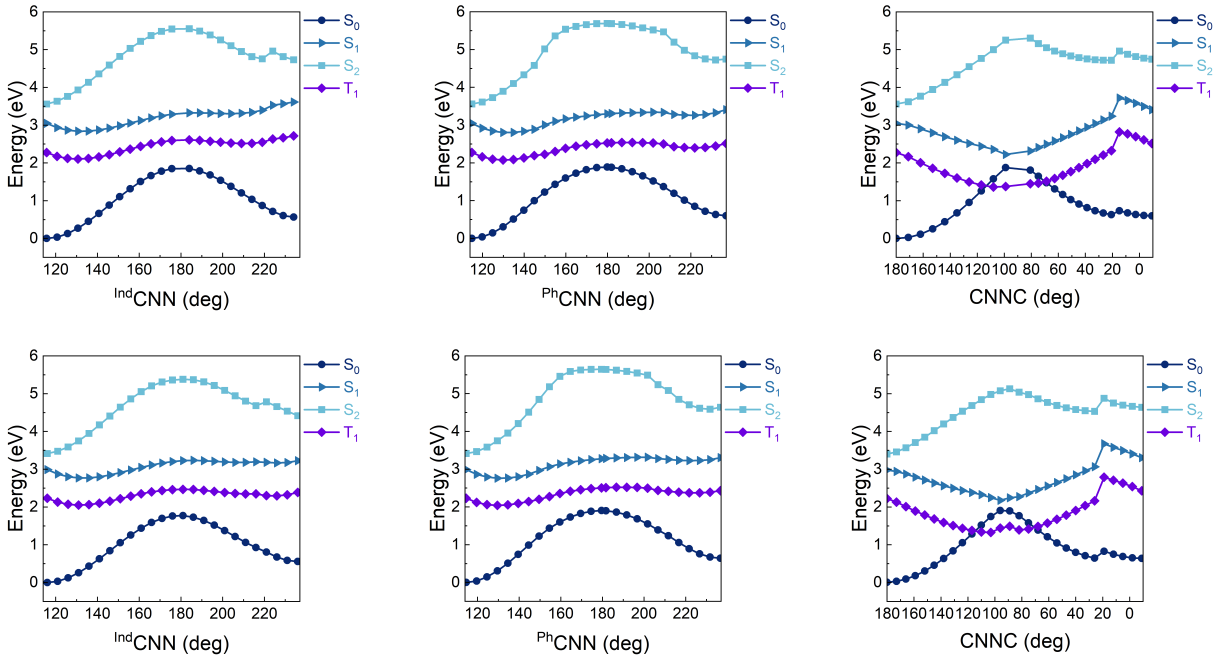


Fig. S22: Computed energy curves of the first three singlet and the first triplet states along the three main azo bond degrees of freedom starting from the lowest isomer of each molecule (*anti-trans*). The  $S_0$  geometry is optimized at each point along the curve with only the angle on the x-axis frozen for OMe-PAI (top) and OMe-PAI-Ph (bottom) along CNNC,  $^{Ind}$ CNN, and  $^{Ph}$ CNN. The  $S_1$  and  $S_2$  energies are TDDFT energies and the  $T_1$  energy is a single point SCF calculated from these  $S_0$  geometries at CAM-B3LYP/6-311G(d,p)-D3BJ/PCM(MeCN).

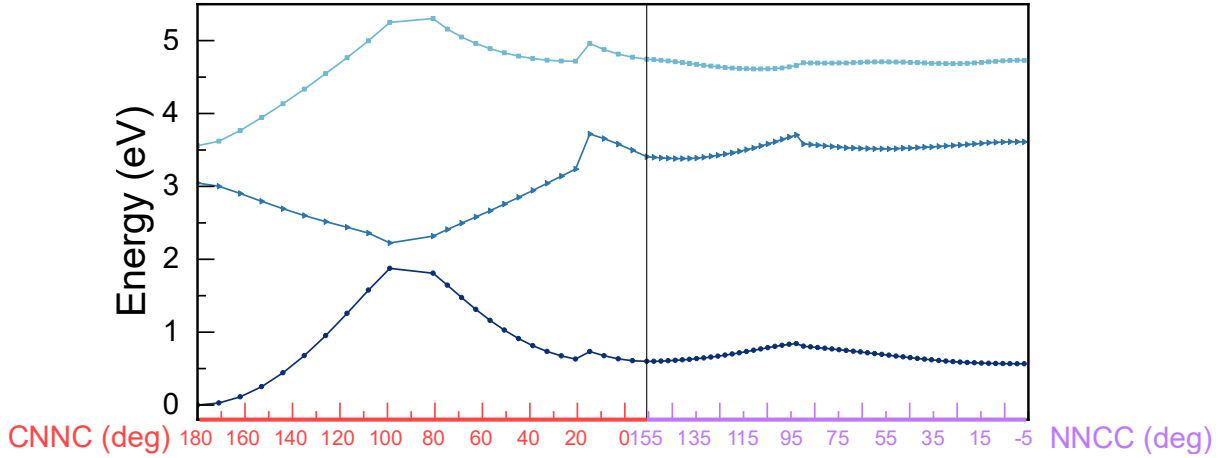


Fig. S23: Combined computed energy curves of the first three singlet states along the CNNC and NNCC dihedral starting from the lowest isomer of OMe-PAI (*anti-trans*) to the same rotamer *cis*, *anti-cis* (vertical line). The higher resolution energy curves starting from *anti-cis*, end near *eclipsed-cis*. The geometry  $S_0$  was optimized at each point along the curve with only the frozen angle on the x-axis, respectively. The  $S_1$  and  $S_2$  energies are TDDFT energies from these  $S_0$  geometries at CAM-B3LYP/6-311G(d,p)-D3BJ/PCM(MeCN).

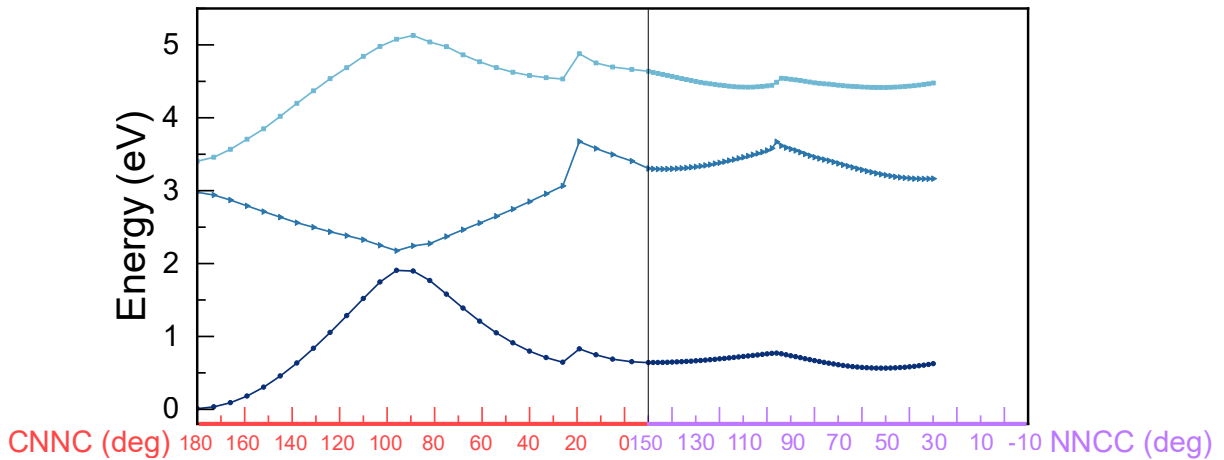


Fig. S24: Combined computed energy curves of the first three singlet states along the CNNC and NNCC dihedral starting from the lowest isomer of OMe-PAI-Ph (*anti-trans*) to the same rotamer *cis*, *anti-cis* (vertical line). The higher resolution energy curves starting from *anti-cis*, end near *eclipsed-cis*. The geometry  $S_0$  was optimized at each point along the curve with only the frozen angle on the x-axis, respectively. The  $S_1$  and  $S_2$  energies are TDDFT energies from these  $S_0$  geometries at CAM-B3LYP/6-311G(d,p)-D3BJ/PCM(MeCN).

## 2.5 Estimated Activation Energies

Activation energies ( $E_a$ ) in the main text were approximated by the energy difference between the *anti-cis* and the lowest energy crossing point on the  $S_0$  PES (Figure 3).  $E_a$  used in the reversion rates were approximated by the energy difference between a *cis*-rotamer and a geometrically accessible transition state. Reversion rates were approximated using transition state theory at 300 K according to the Eyring equation:

$$k_{rev} = \frac{k_B T}{h} e^{-\frac{E_a}{k_B T}}, \quad (1)$$

where  $k_B$  is Boltzmann's constant,  $h$  is Planck's constant, and  $T$  is the temperature. Weighted thermal reversion lifetimes ( $\tau_{rev}^{weighted}$ ) were determined from the sum of the products of the Boltzmann weights at 300 K for each *cis*-rotamer ( $f_{cis}$ ), the Boltzmann weights at 300 K for the transition state activation energies ( $f_{E_a}$ )<sup>4</sup> from the *cis*-isomers to the geometrically accessible transition states, and the unweighted  $\tau_{rev}$  for *cis*-OMe-PAI as

$$\tau_{rev}^{weighted} = \sum_i \frac{P_i}{k_i}, \quad (2)$$

where

$$P = f_{cis} \cdot f_{E_a} \quad \text{and} \quad f_k = \frac{\exp(\varepsilon_k/k_B T)}{\sum_k \exp(\varepsilon_k/k_B T)}. \quad (3)$$

Because no experimental evidence of *eclipsed-cis*-OMe-PAI-Ph was observed experimentally, only the reversion paths from *anti-cis*→*anti-trans* were used in calculation of  $\tau_{rev}^{weighted}$ , i.e.  $f_{cis} = 1$ .

Table S9: Calculated  $E_a$  and approximate thermal reversion rates of OMe-PAI and OMe-PAI-Ph from each optimized transition states (Figure S15-S17) at 300 K along with the Boltzmann weighted (16 decimal float) reversion rate for each isomer.

	Structure	<i>cis</i> -rotamer	Inversion Side	$E_a$ (eV)	$k_{rev}$ (1/s)	$\tau_{rev}$ (s)	$\tau_{rev}^{weighted}$ (s)
OMe-PAI	Figure S13 (a)	<i>eclipsed</i> (0.79) <sup>a</sup>	<i>Ind</i> CNN	1.34	$2.15 \times 10^{-10}$	$4.66 \times 10^9$	$7.37 \times 10^9$
	Figure S13 (d)	<i>eclipsed</i> (0.79) <sup>a</sup>	<i>P<sup>h</sup></i> CNN	1.45	$2.59 \times 10^{-12}$	$3.86 \times 10^{11}$	
	Figure S13 (b)	<i>anti</i> (0.21) <sup>a</sup>	<i>Ind</i> CNN	1.28	$2.09 \times 10^{-9}$	$4.79 \times 10^8$	
	Figure S13 (c)	<i>anti</i> (0.21) <sup>a</sup>	<i>P<sup>h</sup></i> CNN	1.30	$9.37 \times 10^{-10}$	$1.07 \times 10^9$	
OMe-PAI-Ph	Figure S15 (a)	<i>eclipsed</i>	<i>Ind</i> CNN	1.29	$1.47 \times 10^{-9}$	$6.78 \times 10^8$	$8.50 \times 10^{8,b}$
	Figure S15 (c)	<i>eclipsed</i>	<i>P<sup>h</sup></i> CNN	1.57	$3.12 \times 10^{-14}$	$3.21 \times 10^{13}$	
	Figure S15 (b)	<i>anti</i>	<i>P<sup>h</sup></i> CNN	1.52	$1.95 \times 10^{-13}$	$5.14 \times 10^{12}$	
	Figure S15 (d)	<i>anti</i>	<i>P<sup>h</sup></i> CNN	1.27	$2.60 \times 10^{-9}$	$3.85 \times 10^8$	
	Figure S15 (e)	<i>anti</i>	CNNC Rot. <sup>c</sup>	1.30	$9.33 \times 10^{-10}$	$1.07 \times 10^9$	

<sup>a</sup>Boltzmann weight of isomer at 300 K. <sup>b</sup>only *anti-cis*→*anti-trans* paths considered. <sup>c</sup>CNNC rotational transition state.

### 3 TDDFT Tables

Table S10: First 20 TDDFT singlet excitation energies and overlaps of *anti-trans*-OMe-PAI. The HOMO is orbital 70 and LUMO is orbital 71. CAM-B3LYP/6-311G(d,p)-D3BJ/PCM(MeCN).

Excited State	Energy (eV)	Wavelength (nm)	Oscillator Strength	$S^2$	Transitions		
1	3.0705	403.79	0	0	68	$\rightarrow$	71 0.68668
					68	$\rightarrow$	75 0.11316
2	3.5863	345.72	1.1303	0	70	$\rightarrow$	71 0.69456
3	4.6669	265.67	0.0036	0	67	$\rightarrow$	72 -0.11587
					69	$\rightarrow$	71 0.51659
					69	$\rightarrow$	72 -0.12692
					70	$\rightarrow$	72 -0.40589
					66	$\rightarrow$	71 -0.33288
4	4.8178	257.35	0.0235	0	66	$\rightarrow$	75 0.1133
					67	$\rightarrow$	71 0.28209
					67	$\rightarrow$	73 -0.23626
					70	$\rightarrow$	72 -0.11909
					70	$\rightarrow$	73 0.43827
					66	$\rightarrow$	71 0.20908
					67	$\rightarrow$	71 0.4728
5	4.9301	251.48	0.0602	0	67	$\rightarrow$	72 -0.1053
					69	$\rightarrow$	72 0.19471
					70	$\rightarrow$	72 -0.27009
					70	$\rightarrow$	73 -0.22912
					70	$\rightarrow$	74 0.13094
					67	$\rightarrow$	71 0.27247
					67	$\rightarrow$	72 0.12063
6	5.0834	243.9	0.1268	0	69	$\rightarrow$	71 0.44081
					70	$\rightarrow$	72 0.42814
					65	$\rightarrow$	71 -0.11926
					67	$\rightarrow$	71 -0.29276
					67	$\rightarrow$	74 0.18228
					69	$\rightarrow$	71 0.11315
					69	$\rightarrow$	72 0.48233
7	5.3207	233.02	0.0445	0	70	$\rightarrow$	74 0.29015
					66	$\rightarrow$	71 0.56272
					67	$\rightarrow$	73 -0.10039
					70	$\rightarrow$	73 0.39808
					68	$\rightarrow$	72 0.64453
8	5.6758	218.44	0.1644	0	68	$\rightarrow$	73 -0.23762
					65	$\rightarrow$	71 0.45621
					66	$\rightarrow$	73 -0.13761
					67	$\rightarrow$	72 0.14147
					69	$\rightarrow$	72 -0.14416
9	5.9401	208.73	0	0	70	$\rightarrow$	74 0.44037
					68	$\rightarrow$	72 0.22564
					68	$\rightarrow$	72 0.22564
10	6.0201	205.95	0.123	0	65	$\rightarrow$	74 0.44037
11	6.0274	205.7	0.0001	0	66	$\rightarrow$	73 -0.13761

					68	$\rightarrow$	73	0.65848
12	6.2216	199.28	0.3632	0	65	$\rightarrow$	71	0.45427
					69	$\rightarrow$	72	0.3439
					70	$\rightarrow$	74	-0.36776
13	6.4053	193.57	0.0186	0	65	$\rightarrow$	71	-0.1544
					65	$\rightarrow$	72	-0.14332
					66	$\rightarrow$	73	-0.2853
					67	$\rightarrow$	72	0.29162
					67	$\rightarrow$	75	-0.1139
					69	$\rightarrow$	74	-0.24411
					70	$\rightarrow$	72	-0.12262
					70	$\rightarrow$	75	0.4005
14	6.4726	191.55	0.0002	0	65	$\rightarrow$	72	0.23547
					66	$\rightarrow$	73	-0.23264
					67	$\rightarrow$	72	-0.28115
					67	$\rightarrow$	74	-0.12545
					69	$\rightarrow$	74	0.36577
					69	$\rightarrow$	75	-0.10046
					70	$\rightarrow$	72	0.11592
					70	$\rightarrow$	75	0.33403
15	6.6381	186.78	0.0184	0	65	$\rightarrow$	73	0.17762
					67	$\rightarrow$	73	0.59034
					70	$\rightarrow$	73	0.28569
16	6.8238	181.69	0	0	59	$\rightarrow$	71	0.10243
					60	$\rightarrow$	71	0.1021
					61	$\rightarrow$	71	0.10722
					63	$\rightarrow$	71	-0.20275
					68	$\rightarrow$	74	0.38266
					68	$\rightarrow$	75	0.48278
					68	$\rightarrow$	94	0.10822
17	6.9085	179.47	0.7569	0	66	$\rightarrow$	73	0.33472
					67	$\rightarrow$	72	0.38632
					69	$\rightarrow$	74	0.40615
					70	$\rightarrow$	75	0.14022
18	6.9291	178.93	0.0033	0	67	$\rightarrow$	76	0.14581
					67	$\rightarrow$	77	-0.11897
					70	$\rightarrow$	76	0.63625
					70	$\rightarrow$	77	0.10899
					70	$\rightarrow$	79	-0.12916
19	7.0307	176.35	0.3736	0	66	$\rightarrow$	73	0.43736
					67	$\rightarrow$	72	-0.2278
					69	$\rightarrow$	74	-0.26303
					70	$\rightarrow$	75	0.36213
20	7.0985	174.66	0.0152	0	67	$\rightarrow$	76	-0.16649
					67	$\rightarrow$	77	-0.13778
					70	$\rightarrow$	76	-0.12948
					70	$\rightarrow$	77	0.57963
					70	$\rightarrow$	78	-0.17689

70 → 81 0.10691

Table S11: First 20 TDDFT singlet excitation energies and overlaps of *anti-trans*-OMe-PAI. The HOMO is orbital 90 and LUMO is orbital 91. CAM-B3LYP/6-311G(d,p)-D3BJ/PCM(MeCN).

Excited State	Energy (eV)	Wavelength (nm)	Oscillator Strength	$S^2$	Transitions		
1	3.0114	411.71	0.0009	0	88	→	91 0.63762
					88	→	92 -0.15459
					89	→	91 -0.16708
2	3.4411	360.3	0.9715	0	90	→	91 0.69128
3	4.4611	277.92	0.0302	0	87	→	92 0.10662
					88	→	91 0.13595
					89	→	91 0.5597
					90	→	92 -0.33052
					87	→	91 -0.19779
4	4.6086	269.03	0.5548	0	88	→	91 0.10064
					89	→	91 0.30676
					89	→	92 0.13357
					90	→	92 0.54183
					85	→	91 0.20425
					86	→	91 0.28957
					87	→	91 -0.11881
5	4.8172	257.38	0.0311	0	87	→	94 0.23309
					90	→	92 -0.1252
					90	→	94 0.47648
					86	→	91 0.1022
					87	→	91 0.5792
					87	→	92 -0.1117
					89	→	91 0.14112
6	4.9422	250.87	0.0839	0	89	→	92 -0.14091
					90	→	92 0.16468
					84	→	93 -0.22972
					85	→	91 0.27419
					85	→	92 0.18744
					85	→	95 0.13755
					86	→	91 -0.17579
7	5.1736	239.65	0.0064	0	86	→	92 -0.142
					88	→	92 -0.10711
					89	→	92 0.1664
					89	→	93 0.20612
					90	→	93 0.35667
					84	→	91 0.11897
					86	→	91 0.1035
8	5.1848	239.13	0.0286	0	87	→	91 0.24603
					87	→	96 -0.14957
					88	→	92 0.144

						89	→	91	-0.11428
						89	→	92	0.4163
						89	→	95	-0.20462
						90	→	96	0.24458
9	5.4638	226.92	0.0656	0	87	→	95	-0.13642	
					89	→	92	0.1944	
					90	→	95	0.60664	
10	5.5182	224.68	0.0207	0	84	→	91	0.17988	
					88	→	91	0.16015	
					88	→	92	0.5229	
					89	→	92	-0.19021	
					90	→	93	0.26731	
					90	→	95	0.10371	
11	5.6209	220.58	0.1184	0	84	→	91	-0.13514	
					85	→	91	0.25527	
					86	→	91	0.46794	
					90	→	93	0.12951	
					90	→	94	-0.35613	
12	5.6521	219.36	0.0365	0	84	→	91	-0.17373	
					85	→	91	-0.38752	
					86	→	91	0.16462	
					88	→	92	-0.13818	
					90	→	93	0.43609	
					90	→	94	0.12643	
					90	→	95	-0.11321	
13	5.6681	218.74	0.1797	0	84	→	91	0.54112	
					86	→	91	0.13997	
					88	→	92	-0.28713	
					89	→	92	-0.12516	
					90	→	93	0.14086	
14	5.9398	208.74	0.1738	0	83	→	91	-0.31961	
					84	→	91	-0.16022	
					86	→	94	0.10813	
					87	→	92	0.18447	
					89	→	92	-0.2094	
					90	→	96	0.45022	
15	5.9659	207.82	0.0048	0	88	→	94	0.65254	
					89	→	94	-0.17309	
16	6.0697	204.27	0.0189	0	83	→	91	0.34243	
					84	→	91	-0.12736	
					84	→	93	0.1903	
					85	→	91	0.26817	
					85	→	92	-0.17052	
					85	→	95	-0.12284	
					86	→	91	-0.1817	
					86	→	92	0.11207	
					89	→	92	-0.13092	
					89	→	93	-0.21512	

						89	$\rightarrow$	95	-0.14454
						90	$\rightarrow$	93	0.15767
17	6.0955	203.4	0.0578	0	83	$\rightarrow$	91	0.39847	
					84	$\rightarrow$	91	-0.12281	
					84	$\rightarrow$	93	-0.14532	
					85	$\rightarrow$	91	-0.21453	
					85	$\rightarrow$	92	0.11624	
					86	$\rightarrow$	91	0.16556	
					89	$\rightarrow$	92	-0.2056	
					89	$\rightarrow$	93	0.16475	
					89	$\rightarrow$	95	-0.15595	
					89	$\rightarrow$	96	0.10253	
					90	$\rightarrow$	93	-0.11928	
					90	$\rightarrow$	96	0.14908	
18	6.2473	198.46	0.1927	0	83	$\rightarrow$	91	0.13039	
					83	$\rightarrow$	92	0.15967	
					85	$\rightarrow$	93	-0.19602	
					86	$\rightarrow$	93	0.13931	
					87	$\rightarrow$	92	-0.24973	
					89	$\rightarrow$	95	0.38005	
					89	$\rightarrow$	96	-0.1032	
					90	$\rightarrow$	96	0.32049	
19	6.3582	195	0.0099	0	83	$\rightarrow$	91	0.14062	
					83	$\rightarrow$	95	0.10871	
					84	$\rightarrow$	91	0.12376	
					84	$\rightarrow$	92	-0.23105	
					85	$\rightarrow$	93	-0.16458	
					86	$\rightarrow$	94	0.12703	
					87	$\rightarrow$	92	0.37888	
					87	$\rightarrow$	96	0.10529	
					88	$\rightarrow$	93	0.13154	
					89	$\rightarrow$	95	0.1694	
					89	$\rightarrow$	96	0.14096	
					90	$\rightarrow$	95	-0.12819	
					90	$\rightarrow$	97	-0.158	
					90	$\rightarrow$	98	0.14883	
20	6.4082	193.48	0.0297	0	83	$\rightarrow$	91	-0.11047	
					84	$\rightarrow$	92	-0.15651	
					85	$\rightarrow$	93	-0.13429	
					85	$\rightarrow$	94	-0.20017	
					86	$\rightarrow$	93	0.15354	
					86	$\rightarrow$	94	-0.23634	
					88	$\rightarrow$	93	0.12934	
					89	$\rightarrow$	96	0.20736	
					90	$\rightarrow$	97	0.31418	
					90	$\rightarrow$	98	-0.29388	

## References

- [1] N. A. Simeth, A. Bellisario, S. Crespi, M. Fagnoni and B. König, *The Journal of Organic Chemistry*, 2019, **84**, 6565–6575.
- [2] B. Babür, N. Seferoğlu, E. Aktan, T. Hökelek, E. Şahin and Z. Seferoğlu, *Dyes and Pigments*, 2014, **103**, 62–70.
- [3] M. J. Frisch, G. W. Trucks, H. B. Schlegel, G. E. Scuseria, M. A. Robb, J. R. Cheeseman, G. Scalmani, V. Barone, G. A. Petersson, H. Nakatsuji, X. Li, M. Caricato, A. V. Marenich, J. Bloino, B. G. Janesko, R. Gomperts, B. Mennucci, H. P. Hratchian, J. V. Ortiz, A. F. Izmaylov, J. L. Sonnenberg, D. Williams-Young, F. Ding, F. Lipparini, F. Egidi, J. Goings, B. Peng, A. Petrone, T. Henderson, D. Ranasinghe, V. G. Zakrzewski, J. Gao, N. Rega, G. Zheng, W. Liang, M. Hada, M. Ehara, K. Toyota, R. Fukuda, J. Hasegawa, M. Ishida, T. Nakajima, Y. Honda, O. Kitao, H. Nakai, T. Vreven, K. Throssell, J. J. A. Montgomery, J. E. Peralta, F. Ogliaro, M. J. Bearpark, J. J. Heyd, E. N. Brothers, K. N. Kudin, V. N. Staroverov, T. A. Keith, R. Kobayashi, J. Normand, K. Raghavachari, A. P. Rendell, J. C. Burant, S. S. Iyengar, J. Tomasi, M. Cossi, J. M. Millam, M. Klene, C. Adamo, R. Cammi, J. W. Ochterski, R. L. Martin, K. Morokuma, O. Farkas, J. B. Foresman and D. J. Fox, 2016, Gaussian 16, Gaussian, Inc., Wallingford CT.
- [4] J. Calbo, C. E. Weston, A. J. P. White, H. S. Rzepa, J. Contreras-García and M. J. Fuchter, *Journal of the American Chemical Society*, 2017, **139**, 1261–1274.